AIAA JOURNAL
Vol. 43, No. 3, March 2005

# High-Speed Digital-Particle-Image-Velocimetry Study of Vortex Breakdown

Sandra M. Klute*
*Luna Innovations, Blacksburg, Virginia 24060*
and
Pavlos P. Vlachos† and Demetri P. Telionis‡
*Virginia Polytechnic Institute and State University, Blacksburg, Virginia 24061*

**Time-resolved digital particle image velocimetry is employed to investigate the flowfield along a plane passing through the axis of a delta-wing leading-edge vortex. A sampling frequency of 500 Hz allows the detailed documentation of the temporal evolution of the field. Spiral vortex breakdown is studied in terms of velocity and vorticity fields along a plane through the vortex axis. The sense of vorticity is reversed at the onset of vortex breakdown, in agreement with earlier experimental and numerical results. Evidence is now provided that periodic oscillations observed earlier are attributed to a rotating and expanding spiral of the helical vortex breakdown.**

## Nomenclature

| | | |
|---|---|---|
| $C$ | = | model chordlength |
| $f$ | = | frequency |
| plane $X$ | = | plane through the vortex axis and normal to the wing |
| $R_{\text{inst}}$ | = | radius of helical mode instability |
| $Re$ | = | Reynolds number, $U_\infty C/\nu$ |
| $r$ | = | distance from axis of vortex |
| $S$ | = | local semispan |
| $Sr$ | = | Strouhal frequency, $fC/U_\infty$ |
| $U_\infty$ | = | freestream velocity |
| $V_\vartheta$ | = | circumferential velocity |
| $X$ | = | distance along the model chord |
| $Y$ | = | distance normal to the wing surface |
| $\alpha$ | = | angle of attack |
| $\nu$ | = | kinematic viscosity |
| $\tau$ | = | convective timescale, $C/U_\infty$ |

## Introduction

THE flow over a delta wing at an angle of attack is comprised of a complex combination of several distinct organized temporal periodic phenomena. First, instabilities develop in the shear layers emanating from the leading edge. Gad-el-Hak and Blackwelder[1] observed dyes injected near the leading edge to roll into a series of discrete vortices, which form in lines nearly parallel to the leading edge. As these vortices convect with the shear layer, they rotate around each other and finally coalesce to form a single larger vortex. This temporally periodic instability was found to exist at a reduced frequency of $Sr = 10$–$30$, where $Sr = fC/U_\infty$. Payne et al.[2] presented flow visualizations that clearly confirm the existence of secondary structures developing in the leading-edge shear layer. However, the structures they observed appeared to be stationary. Lowson[3] clarified the discrepancy by capturing two distinct instabilities in his flow visualization, a fact that was later confirmed by Reynolds and Abtahi.[4] The photographs confirmed the existence of the two-dimensional, classical Kelvin–Helmholtz shear-layer instabilities, as first observed by Gad-el-Hak and Blackwelder.[1] Toward the apex, the pairing of the instabilities appeared to be suppressed by the stretching and roll-up process sooner than at the trailing edge, where the sheet was frozen at two pairings as it was swept into the vortex and stabilized. In contrast to the results of Gad-el-Hak and Blackwelder,[1] Lowson[3] found a constant Strouhal number over a range of freestream velocities. This frequency was found to be a result of external noise, which proved capable of forcing the entire flowfield at a certain frequency. Lowson[3] observed a second and more obvious locally streamwise instability of the vortex sheet, which gives rise to the steady structures observed by Payne et al.[2] to surround the vortex core. Pressure measurements presented by Payne[5] show the existence of pressure variations in the vortex core that correlate with the observed cell structure. Washburn and Visser[6] performed a detailed study of these structures at angles of attack up to 25 deg, and Schaeffler[7] documented their existence on a 75-deg sweep delta wing at an angle of attack of 38 deg. These streamwise instabilities are thought to be caused by the effects of vortex sheet curvature.

A second type of periodic phenomenon observed in the high-alpha delta-wing flowfield is caused by the streamwise fluctuation of the breakdown location. Gursul and Yang[8] observed periodic oscillations of the breakdown location over a 70-deg sweep delta wing through use of flow visualization and 30 frame/s video cassette recoder and charge-coupled-device (CCD) cameras. They presented the power spectrum of the breakdown location at $\alpha = 26$, 30, and 37 deg, and calculated that most of the energy is concentrated below a dimensionless frequency of $Sr = 0.2$.

Vortex shedding is known to occur over delta wings.[9,10] For a delta wing, vortex shedding is initiated for angles of attack greater than or equal to those for which the breakdown location has reached the apex of the wing. Instead of rolling up over the wing, the shear layers convect downstream for a distance of approximately one wing chord before they roll into vortices, which are then shed periodically to form a Karman type of vortex street pattern. Vortex shedding can be either symmetric or alternate, this being determined by the aspect ratio of the wing. Very little Reynolds-number dependence is exhibited; a nondimensional Strouhal frequency of around 0.2 is found for a 75-deg sweep wing. It is intriguing that this Strouhal number value is equal to the one measured by Gursul et al.[8] for a phenomenon that is different than vortex shedding over a body. In fact, this numerical evidence implies that perhaps there is an underlying common feature in the two phenomena.

Finally, periodic signals in the breakdown region of the leading-edge vortices (LEV) are manifested strongly in the velocity power spectra. Faler and Leibovich[11] were the first to use laser Doppler velocimetry to measure dominant frequencies in the breakdown

Received 12 August 2003; revision received 12 August 2004; accepted for publication 23 August 2004. 

*Research Scientist, Optical Devices Group.
†Assistant Professor, Department of Mechanical Engineering. Member AIAA.
‡F. J. Maher Professor, Department of Engineering Mechanics. Associate Fellow AIAA.

region of bounded columnar vortices. A consensus regarding the origin of these disturbances has not yet been reached, although experimental results appear to be somewhat consistent with respect to frequency. Gursul[12] attributed the oscillations to nonaxisymmetric structures that rotate with the LEV in the breakdown region and in particular to the helical mode instability of the breakdown wake flow.

Although single- and dual-point measurements provide glimpses into the spatially and temporally varying flowfields, the development of particle image velocimetry (PIV) allowed for the first time an additional dimension of insight into these complicated flows. Among the first to use PIV over the delta wing were Atta and Rockwell.[13] In these experiments, a scanning argon-ion laser was used to obtain data at a sampling rate of approximately five times the convective timescale, $\tau = C/U_\infty$. The region of vortex breakdown exhibits a pattern characteristic of the helical or spiral mode, and corresponding contours of azimuthal vorticity switch in sign at the onset of breakdown, in agreement with the theoretical model of Brown and Lopez.[14] Althaus and Brucker[15] used particle-tracking velocimetry to study the instantaneous internal structure of vortex breakdown in a cylindrical tube, for the cases of both spiral and bubble types of breakdown. Their results showed that in the case of the bubble-type breakdown a vortex ring exists at the downstream end of the bubble. This ring is tilted with respect to the axis of the vortex and gyrates around it at a frequency that appears to remain fairly constant. Towfighi and Rockwell[16] and Lin and Rockell[17] were able to obtain PIV data along a plane passing through the axis of delta-wing vortices. They observed the switch in the sign of vorticity and documented in detail the velocity and vorticity fields in the neighborhood of vortex breakdown. Visbal[18] presented in 1995 a thorough review of contributions in this area, including his own numerical results.[19] Since then, more contributions appeared in the literature,[20–22] providing significant information on the structure of vortex breakdown. However, PIV investigations of the phenomenon were limited to a very low range of frequencies.

In the present paper time-resolved, two-dimensional digital-particle-image-velocimetry measurements are presented, which document the flowfield over a 75-deg-sweep delta wing at a 40-deg angle of attack. The data presented here were taken at frequencies two orders of magnitude greater than any reported in the literature to date. This allows us to examine the temporal evolution of vortex breakdown in the form of instantaneous sectional streamlines and vorticity contours and to provide for the first time noninvasive spectral information in the breakdown region. It is thus possible to trace accurately the source of the oscillating signals and the corresponding frequencies and connect them to the temporally evolving flow patterns.

## Experimental Configuration

Measurements were obtained over a 75-deg sweep delta wing at an angle of attack of 40 deg in the Engineering Science and Mechanics Department (ESM) water tunnel. This facility has a test section of $61 \times 61$ cm and can reach a maximum speed of 1 m/s with turbulence levels less than 1%. The model had a chordlength of 14.1 cm, and the freestream velocity was set at 32 cm/s, yielding a Reynolds number based on the wing chord of $Re = 4.5 \times 10^4$. A 40-W copper-vapor pulsing laser was used, delivering 50 mJ per exposure. Optical components were employed, as shown in Fig. 1 to generate a 1-mm-thick laser sheet, which was oriented along the core of the vortex and normal to the model wing. We will refer to the plane of the vortex sheet as plane $X$. Dye flow visualizations and earlier experiments of the present group indicated that the leading-edge vortex over a wing with this sweep is inclined by 6.4 deg with respect to the leading edge. Plane $X$ was given the same inclination.

A high-speed CCD camera (EG&G MD4256) was used. The laser was synchronized with the camera using a timer board (Real Time Devices, TC524). The number of images acquired was 500/s with a resolution of $256 \times 256$ pixels. Digital images were automatically stored in the image buffer of a SB4001 Adaptive Optics frame grabber. Hollow glass silver-coated spheres of 10–30 $\mu$ average diameter were used as flow tracers. The particle population density was on the order of 0.02 particles/px.

Calibration was performed in order to compensate for image distortion caused by light refractions. The magnification was adjusted so that the field of view was a square of $6.68 \times 6.68$ cm. To temporally resolve structures developing in the breakdown region, images were recorded at a rate of 500 frames per second, yielding a time interval between frames of 0.002 s. The convective timescale of the flow $\tau$ was 0.44 s. Therefore, data were taken at 0.5% of one convective timescale apart, a speed capable of providing very good temporal resolution of any structures that could be responsible for the frequencies measured in the breakdown flowfield. Data were obtained over a period of 4 s.

The processing of the recorded images was carried out using a software package based on the principles described by Willert and Gharib[23] and Westerweel.[24] Dual-frame cross-correlation was employed, with square interrogation regions of $16^2$ pixels and 75% overlapping, resulting to a total of $61 \times 61$, or 3721 vectors for each instant. Subpixel accuracy in the velocity estimation was achieved using a standard, three-point, Gaussian-fit, peak-detection

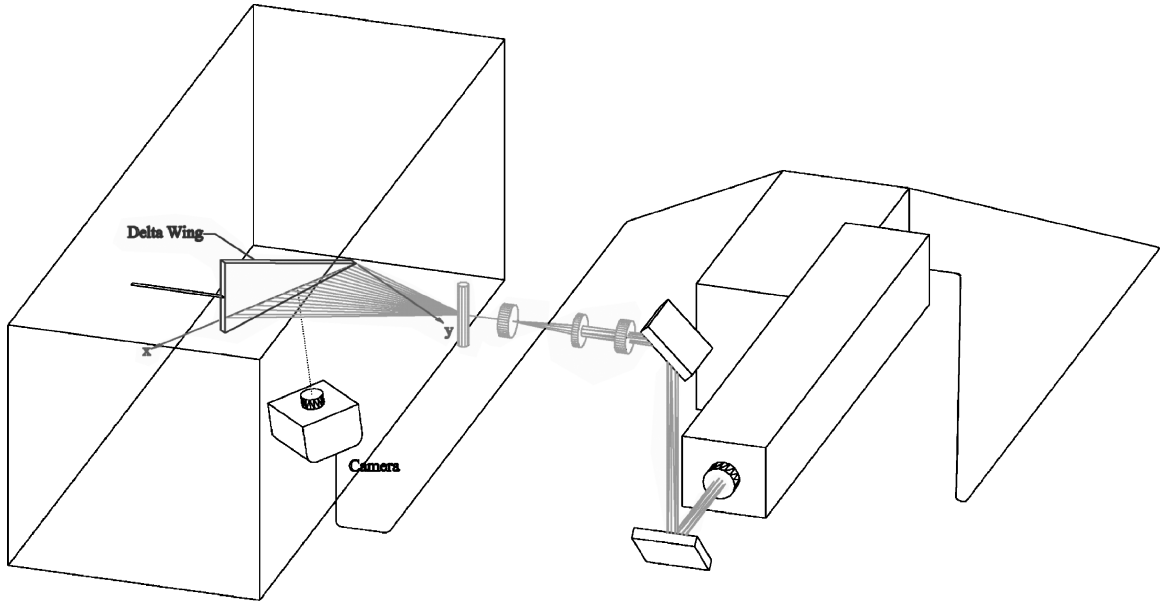


**Fig. 1 Particle image velocimetry configuration for ESM water tunnel.**

algorithm, resulting to an accuracy of 10% of the pixel size. This corresponds to uncertainty of the velocity estimation in the order of 2% with respect to the maximum velocities recorded. However this error is expected to increase as the velocity decreases, as reported by Huang and Gharib.[25] The use of the CCD camera removes the effect of digitization errors and provides superior signal-to-noise ratio. Moreover, by seeding the flow with neutrally buoyant hollow glass spheres, errors related to seeding are minimized, as found by Angui and Jimenez.[26]

## Results and Discussion

The nondimensional component of the vorticity normal to the measurement plane was calculated from the recorded velocity data using implicit, compact, fourth-order finite differences in order to minimize the effect of the truncation error in the computation. The velocity and vorticity fields were analyzed using a scientific visualization package. Animations of the time-resolved data were thus generated. Because of the enormity of the amount of the information generated, we present here only a few instantaneous frames.

To aid in the understanding of the physics, we provide in Fig. 2a numerical results of Visbal,[18] presenting a constant vorticity surface in the neighborhood of breakdown. Helical vortex breakdown is characterized by vortex tubes forming a helix, very similar to a corkscrew, beautifully predicted by the numerical calculations. The onset of helical vortex breakdown can be defined as the location where the core of the vortex deviates from a straight line emanating from the apex. The numerical results indicate that this deviation could be sharp, forming a kink of the vortex tube. Visbal has also cut the domain by a plane passing through the vortex initial core and normal to the wing, as shown in Fig. 2a. This is the plane we call plane $X$ and is the same with the plane along which we obtained our data. The spiraling vortex core pierces plane $X$ alternately, coming up out of the plane and then going back down into it. It should be emphasized that vorticity fields are best represented in terms of vortex lines, but vortex surfaces are easier to present and visualize in three dimensions. To help with our subsequent discussion, we provide in Fig. 2b a sketch of the vortex lines contained in the $\omega = \text{const}$ surface of Fig. 2a. Many earlier experimental investigations have indicated that the vortex lines form helices reminiscent of braids. And in Fig. 2c, we present a cut of the configuration of Fig. 2a by plane $X$.

Frames of measured velocity vectors with some superimposed streamlines along plane $X$ are presented in Fig. 3. The frame of the data in plane $X$ had its leading boundary a certain distance downstream of the apex as noted in the dimensionless coordinates. Evident in almost every frame is the development of a vortex pattern that is asymmetric and characteristic of the helical mode of vortex breakdown. It should be emphasized that the streamlines displayed are lines tangent to the vector components in this plane and not the projections on this plane of streamlines in space. Similar patterns were reported in Refs. 15 and 17.

The breakdown in our results appears to be initiated by a sudden divergence of the streamwise velocity vectors approximately at $X/C = 0.5$. Because the streamlines were spatially set in each frame to resolve the interior of the breakdown region, and then integrated both forward and backward within plane $X$, the concentration of lines upstream of breakdown identify the core of the vortex, and their divergence clearly indicates the onset of breakdown. The frames of Fig. 3 indicate that the flow feeding into the breakdown area is undulating in the vertical direction. Deviations as much as a nondimensional distance of $Y/C = 0.03$ can be observed.

We note that a uniformly spiraling flow, that is, axisymmetric flow would not result in the undulations documented here. Rather, the motion captured in Fig. 3 is the result of the helical mode instability. Slight oscillations of the instantaneous streamlines leading up to the breakdown location can also be seen in some of the data published by Rockwell.[27] The series of images presented in the frames of Fig. 3 illustrate the development of the flow captured at only three instances at $\tau = 0$, 0.18, and 0.36. The reader can find in Ref. 28 the complete sequence of these frames spaced apart by $\tau = 0.9$, as well as an animation of the field. Reference 28 is the Ph.D. dissertation of the

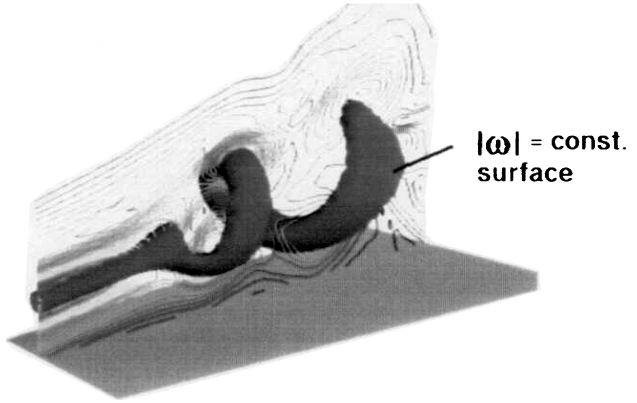


**Fig. 2a Computational results of Visbal[18] presenting the core of a vortex in the neighborhood of vortex breakdown.**

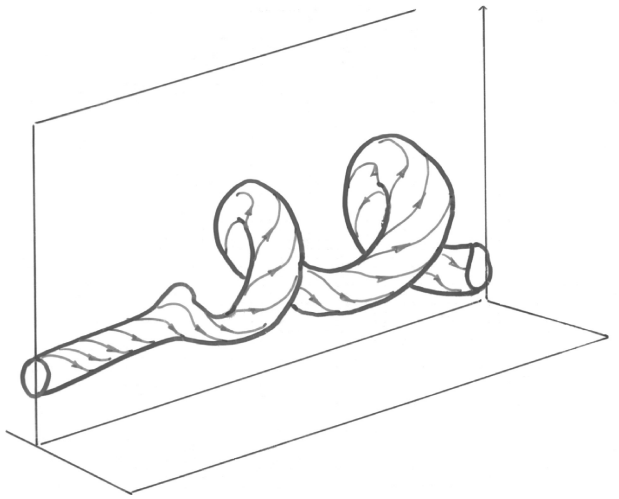

**Fig. 2b Schematic of the core of Fig. 2a, showing vortex lines.**

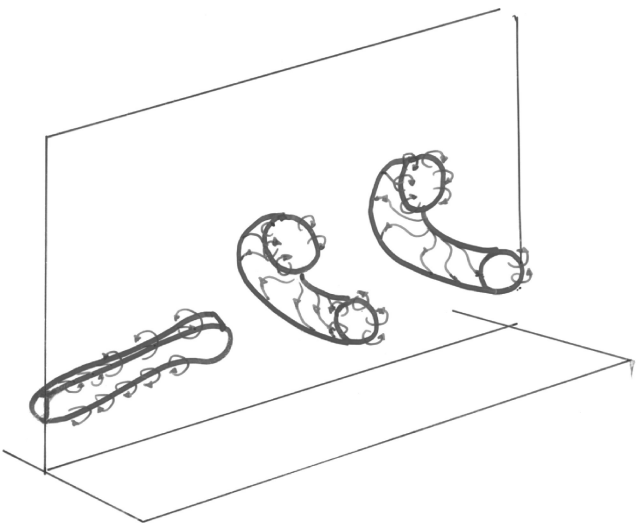

**Fig. 2c Schematic of a cut by plane $X$ of the core shown in Fig. 2b.**

first author and is available electronically at http://www.lib.vt.edu/. One needs to click on "VT Electronic Dissertations" and then search for the author's name.

Analyzing the sequence of instantaneous flowfields allows us to track the evolution of the helical instability, assuming that it is within the frequency range previously documented. Evident in the first figure are three distinct structures, labeled A, B, and C, following the first two kinks of the vortex core. We will refer to them as vortex A, vortex B, and vortex C, even though they are not individual

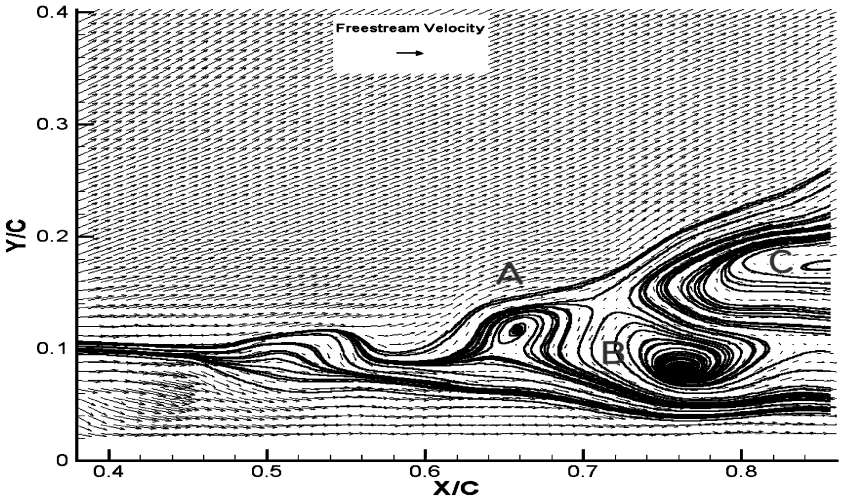


**Fig. 3a Vortex breakdown time series, $\tau = 0$.**

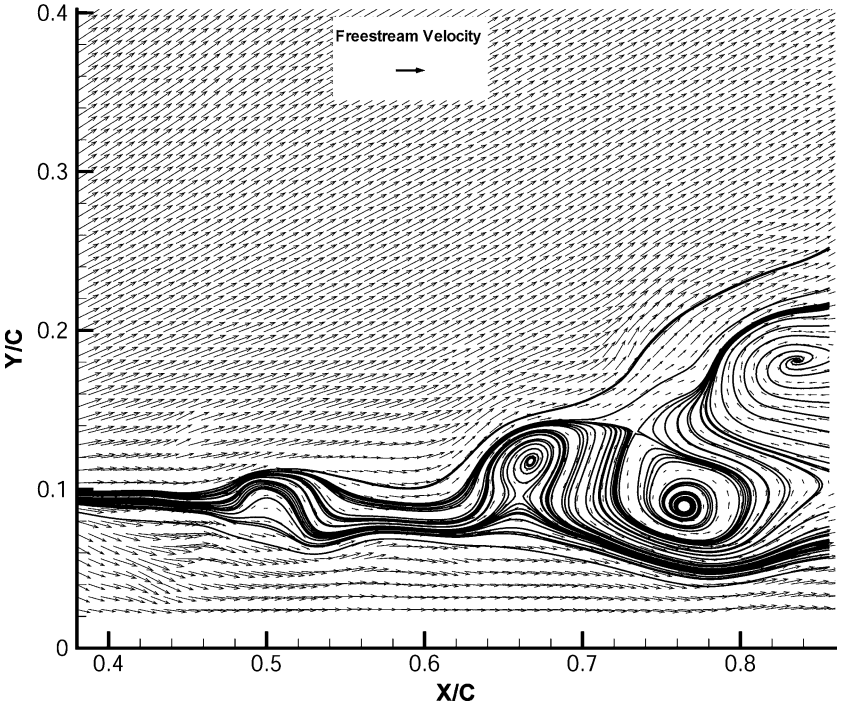


**Fig. 3b Vortex breakdown time series, $\tau = 0.018$.**

vortices, as explained in the following. These structures have alternating senses of rotation, which confirms the fact that they belong to the same helical vortex, a fact observed earlier by other investigators.[15,17,19] These are sections of the same vortex tube, cut by plane $X$ as schematically indicated in Fig. 2c. We also observe that all three patterns are stable nodes, that is, they are spiraling inward. This indicates that the vortex is entraining flow from its surroundings.

Employing the first 10 instantaneous frames at our disposal (not shown here), we were able to track these structures in time and estimate their position in plane $X$. Streamline structures are not invariant to the system of coordinates, a fact that influences the results if vortical patterns are propagating. However, the centers of vortices or vortical sections as captured by streamline patterns are invariant to the system of coordinates. In Fig. 4 the vortices displace in the streamwise direction and were tracked for a period of $\Delta\tau = 0.9$. At the last frame (not shown here) one of the vortices has convected out of the measurement region. In this figure the nondimensionalized time is plotted vs the nondimensionalized chordwise distance of the center of each vortex. Over the time period plotted, vortex A is convected downstream at an almost constant rate for the first seven time steps. It then moves slightly upstream to be convected again back downstream at the previous rate. Study of the images corresponding to these time steps shows that the jump back in position correlates with increasing strength of a region to the right of the vortical structure that is feeding into and around the next structure. In fact, as time goes on, this imprint of the vortex grows stronger until vortex A disappears altogether and is replaced by an unstable node, one that is spiraling outward. Coinciding with this development, a new structure appears to the left of vortex A. This too is an unstable node. However, the next time step represents a stabilizing effect for the new vortex as it now spins inward. Note that in the last frame of this series the vortices now centered at $X/C = 0.68$ have switched their vertical orientation as well as their rotational sense in comparison to the original structures. The helical vortex filament appears to have rotated through a portion of its period, by an angle large enough to pierce plane $X$ from the opposite normal direction. This implies that the helix is rotating as a rigid body, in the same sense with the vorticity of the initial core of the vortex. In other words the "corkscrew is turning."

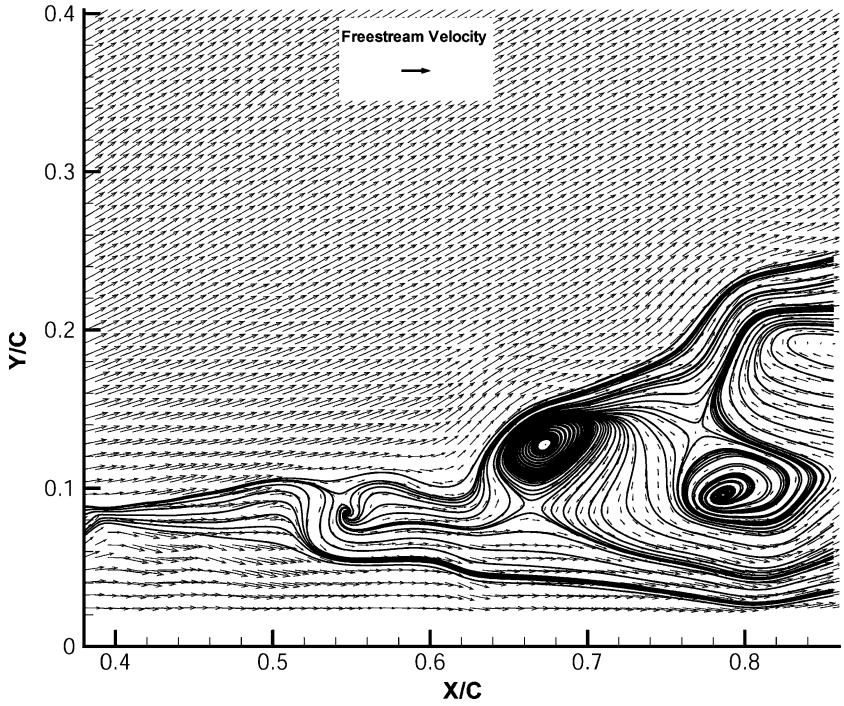


**Fig. 3c Vortex breakdown time series, $\tau = 0.036$.**

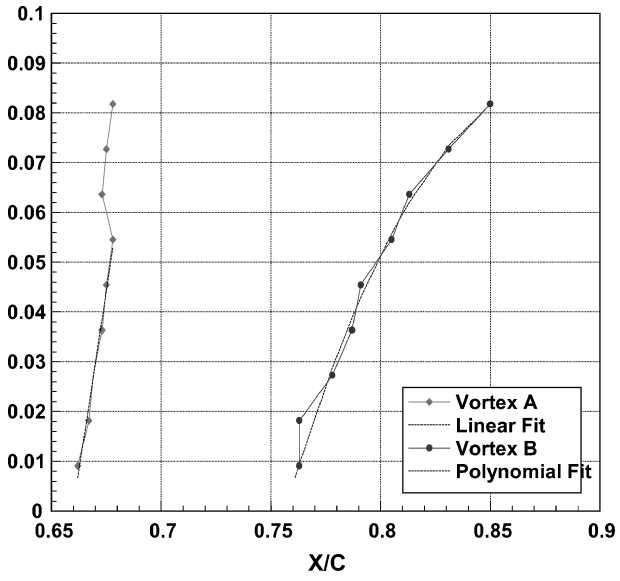


**Fig. 4 Convection of helical mode instability over short distance.**

A final point to note with respect to this series of frames is the convection speed of the second vortex tracked, vortex B, which moves at a faster rate than vortex A. Not only is the speed of downstream propagation of the vortex greater, but also it appears to be accelerating downstream. These results are consistent with Visbal's finding[19] that the radius and wavelength of the instability are expanding with downstream distance. In other words, the spiral of the vortex core is stretching in the downstream direction.

The traditional approach to characterizing the unsteadiness in the breakdown wake flowfield involves power spectra of either velocity or pressure. One of the goals of this investigation is to link these more traditional representations to the quantitative global instantaneous velocity data that were just presented. Taking advantage of our capability to capture and store images at such high frame rates, we calculate the fast fourier transform (FFT) of the axial velocity component throughout the measurement plane. For these calculations, the full 500-Hz data set was used over 4 s. In Fig. 5a we present the time record of the $U$-velocity component along with the FFT of the signal for a location $(X/C, Y/C) = (0.8, 0.048)$. Because the data were obtained over one 4-s time interval only, we anticipate that any quasi-periodicity would not be discernible in the FFT. A first glance at this figure confirms this expectation; however, further study shows some interesting results. This location is at the edge of the envelope containing the helical vortex, and the velocity is oscillating around a mean value that is slightly less than that of the freestream. The time record shows fairly rapid velocity fluctuations, and the FFT of the signal appears noisy as well. We notice first a concentration of energy below 1 Hz. There is a perceptible peak, at 4.2 Hz and then a more broadband region of energy concentrated around 10 Hz. The following frames present similar data along a line normal to the surface of the model between $(X/C, Y/C) = (0.8, 0.096)$ and $(X/C, Y/C) = (0.8, 0.144)$ at equal intervals. As we progress further into the broken-down vortex, the time record shows values oscillating around lower mean values. An interesting feature of these records is that the average time between large oscillations is increasing with distance into the vortex. In Fig. 5b, a fairly distinct peak is now evident in the FFT at approximately 6.3 Hz. In Fig. 5c, two new peaks at 1 and 3.9 Hz have emerged, which are most dominant at this location. The corresponding time records clearly show excursions ranging between 0.7 and $-0.5$. The frequency of 3.9 Hz appears consistently in all power spectra and has a large amount of energy centered around it. For this most dominant frequency of 3.9 Hz, the corresponding Strouhal number is $Sr = 1.7$. Further increase in distance away from the surface of the model brings us towards the top of the vortex, and the periodicity becomes buried in a noisier signal. Although these spectra were calculated without any averaging and are to be interpreted with caution, when they are considered together with the animation, they offer better understanding of the origin of certain oscillations in the flowfield.

The dominant frequency shown in the spectra just presented is approximately 3.9 Hz. This corresponds to a Strouhal frequency of $Sr = 1.72$, which is very close to that found in the literature[18,19] for this chordwise location. It would be interesting to examine the variation in frequency along a ray of the vortex. Because slower flow is found in the broken-down flowfield of the vortex, we can use a velocity criterion to establish the size of the core region. Taking this to be approximately $0.85\,U_\infty$, the averaged location that defines the vortex region is contained between the dashed lines in Fig. 6. This

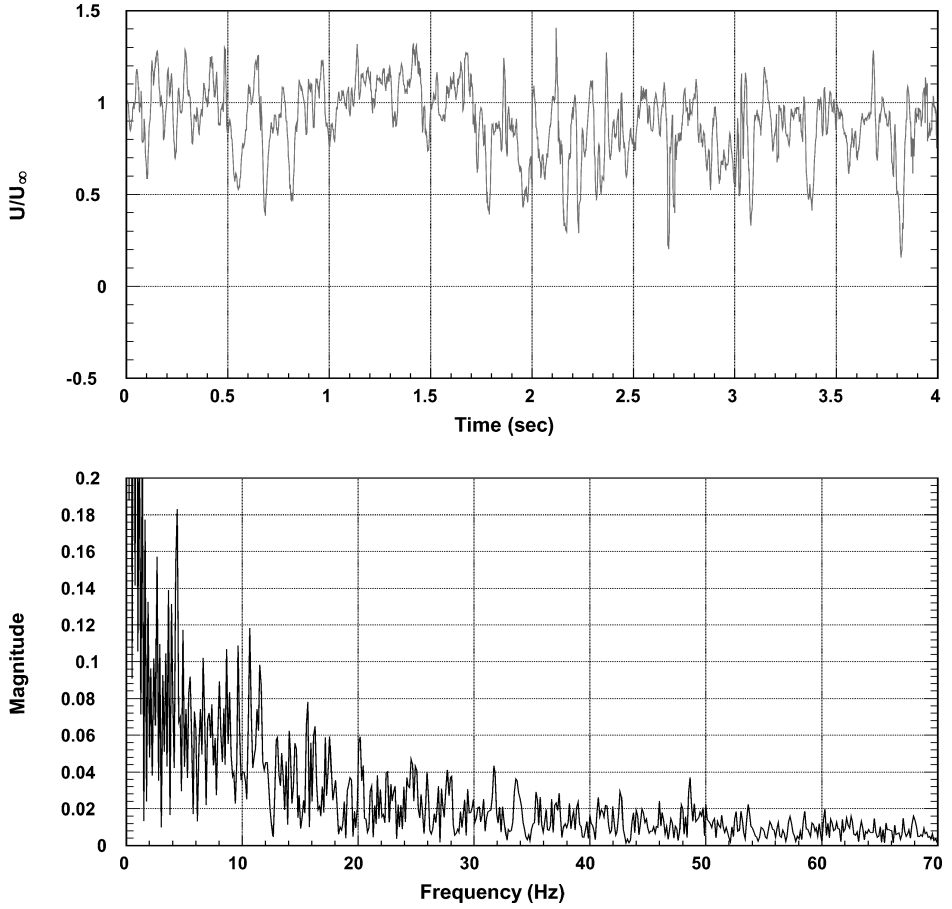


**Fig. 5a Time record and FFT of $U$-velocity component; $(X/C, Y/C) = (0.8, 0.048)$.**

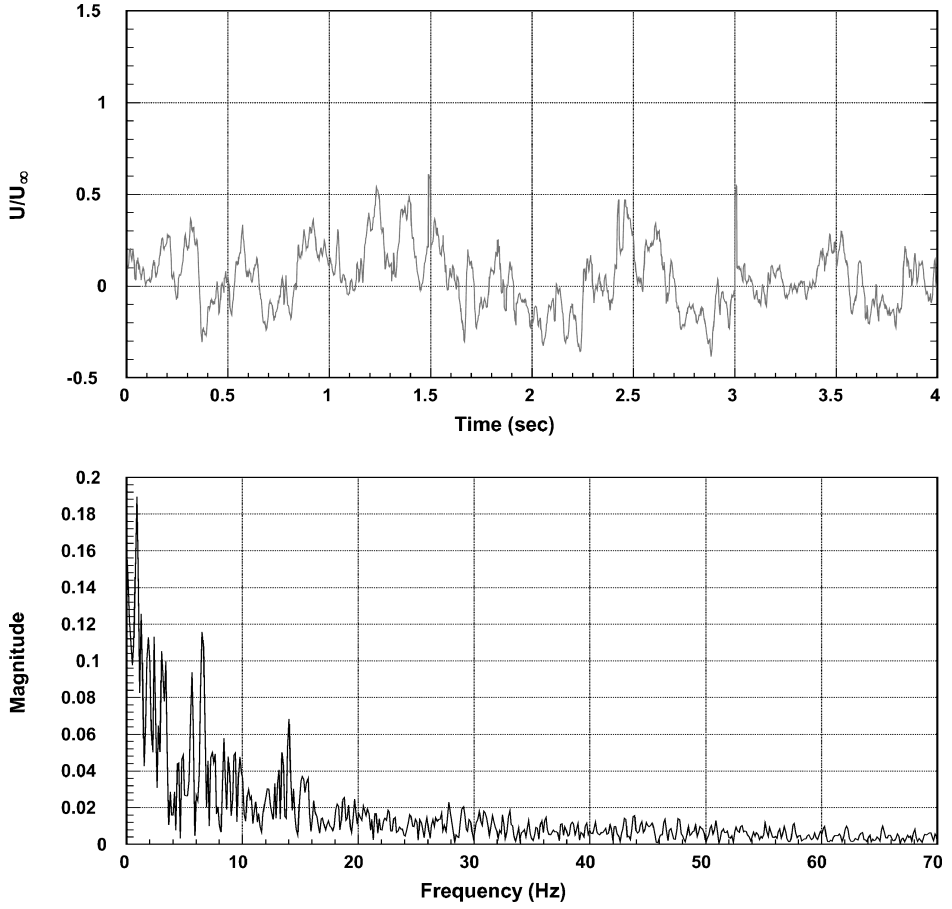


**Fig. 5b Time record and FFT of $U$-velocity component; $(X/C, Y/C) = (0.8, 0.096)$.**

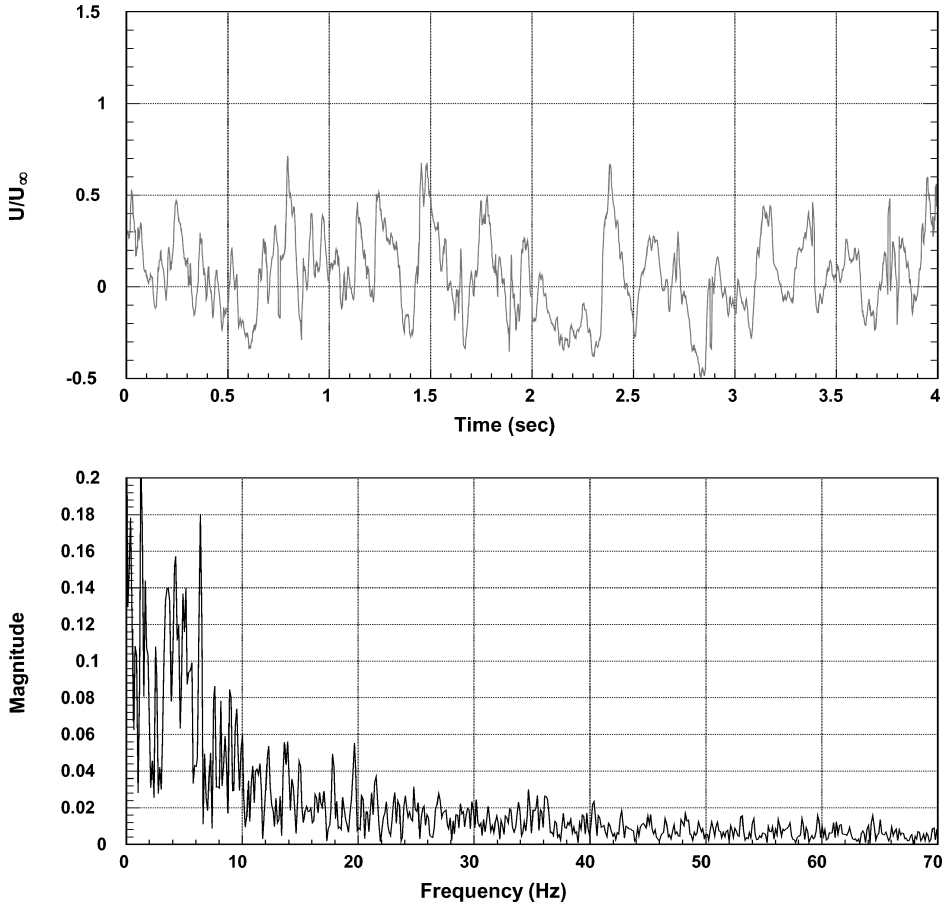


**Fig. 5c Time record and FFT of *U*-velocity component; (*X/C*, *Y/C*) = (0.8, 0.144).**

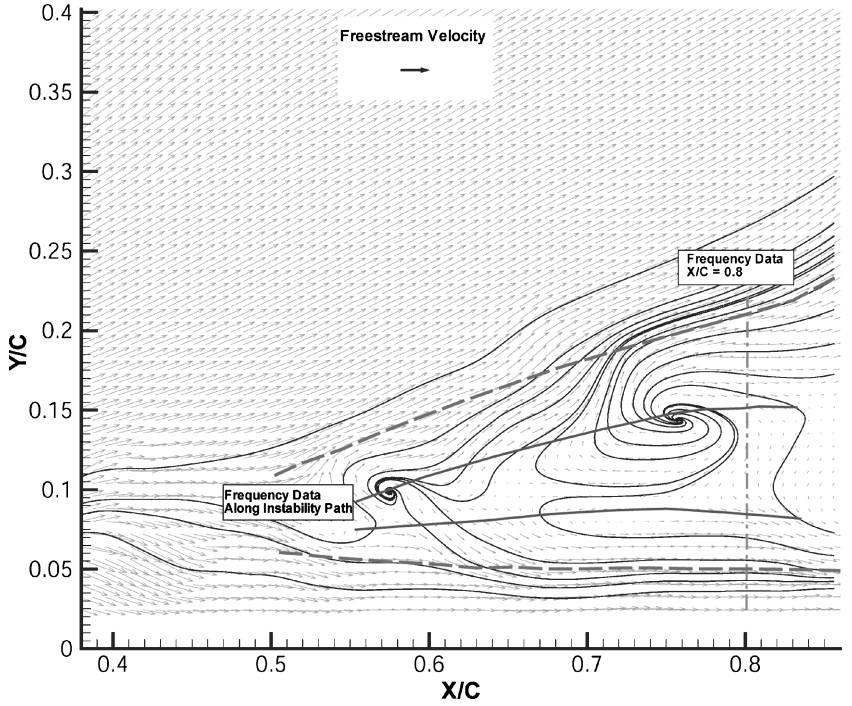


**Fig. 6 Trajectory of helical mode instability.**

envelope was defined based on all of the frames available to us, but it is drawn on just one of the instantaneous frames of streamlines. The two solid lines shown in this figure represent the paths of the centers of counter-rotating structures as they displace within the measurement plane. These structures tracked very consistently over the 4-s time record. The variation in frequency with the chordwise direction was studied at points lying on the trajectory of the instability because it was for this region at $X/C = 0.8$ that the FFT showed most definition. The results are presented in Fig. 7, where we plot the nondimensional frequency vs chordwise location along the trace of the helix. The solid curve in this figure is a least-squares fit of the data. The dominant downstream frequency of approximately 4 Hz remains evident throughout each of the FFTs. However, the energy content of higher frequencies increases with upstream progression.

Previous experiments have documented an increase in nondimensional frequency as the breakdown point is approached from the downstream direction.[9,29,30] Here flow visualization was conducted, and the progression of the helical mode instability tracked at 30 Hz in a region covering the first distance $X/C = 0.15$ downstream of breakdown. As was pointed out in this work, the variation of frequency, with distance in the chordwise direction, can be explained by a combination of the following two key points. The first is that the radius of the helical instability $R_{\text{inst}}/X$ grows linearly with axial distance. The second is that the velocity component which convects the helical instability follows a conical pattern, where $V_\theta/U_\infty$ varies linearly with $r/X$. With simple calculations we have shown that for a given angle of attack, the reduced frequency $fX/U_\infty$ is constant. However, this does not agree with the results presented by Rediniotis,[9] or with the frequency data just presented, which both document an increase in reduced frequency with approach toward the apex.

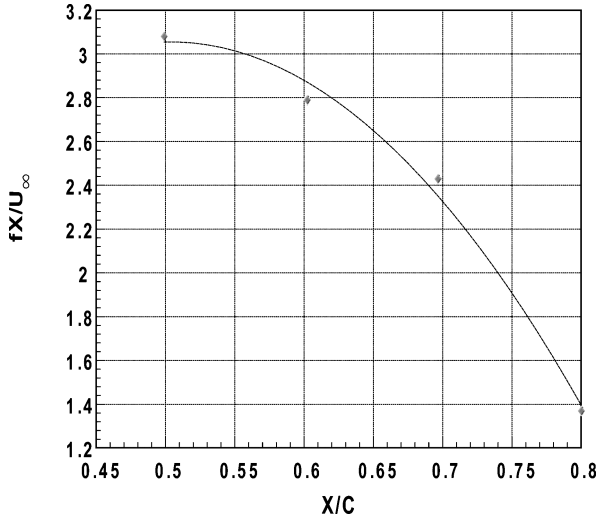


**Fig. 7 Variation of reduced frequency with streamwise location.**

One possible explanation for this discrepancy is that the radius of the helical instability grows with distance downstream of breakdown at a rate faster than $S/X$. Although flow visualization seems to indicate this,[28,29] the data presented here show the trajectory of the instability to expand proportionally with the vortex size and at a rate equal to or smaller than $S/X$. Brucker[31] has documented that in the case of spiral-type breakdown the high radial velocities associated with the deflection of the flow around the stagnation point away from the centerline are responsible for displacing the fluorescein out of the vortex axis. This could possibly explain the appearance of breakdown growing at rates faster than $S/X$, but we are still left with the question on the origin of the high frequencies for $X/C < 0.15$ or higher frequencies downstream of breakdown. Even if the observed dye in the flow visualizations has been displaced off the axis of the vortex, the apparent frequencies observed in the flow visualization correspond to a definite rotating structure. In an attempt to further understand this phenomenon, we calculated the frequency content in the flowfield at a location upstream of breakdown namely at $(X/C, Y/C) = (0.47, 0.09)$. At this location, the power spectrum showed a strong peak at 12.3 Hz, approximately the maximum picked up just downstream of breakdown. This information suggests then that the variation in the frequency of the helical instability close to the breakdown region might be the result of an upstream disturbance that is carried into the breakdown region for the first few rotations. Once the vortex has reached its critical state and broken down, it no longer experiences the direct influence of the upstream disturbance, and the helix is convected as just mentioned with the conical azimuthal vortex velocity approaching a nondimensional frequency of one.

We now turn our attention to the vorticity distributions of this field, which appears as a color animation in Ref. 28. In this paper we only present in Fig. 8 gray-scale vorticity contours at one instant of the flow. The most dominant feature of vorticity distributions is that prior to breakdown the sign of vorticity in the region adjacent to the wing is positive, whereas once breakdown occurs we see consistently negative values next to the wing surface. The same phenomenon occurs with the vorticity in the portion of the vortex furthest away from the wing, where a sign change in the vorticity can also be seen once the vortex breaks down. These results confirm those documented in the literature, namely, a reversal in azimuthal

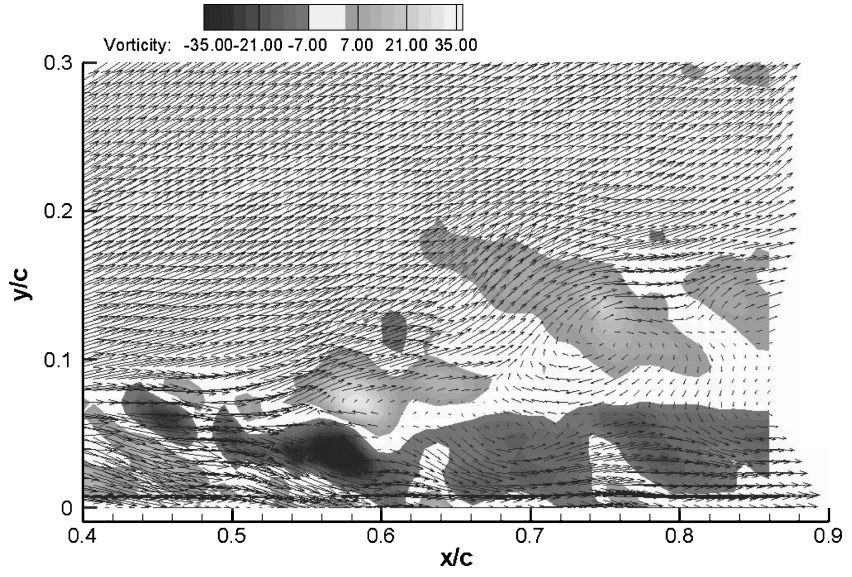


**Fig. 8 Vorticity contours overlaying instantaneous streamlines and velocity vectors for $\tau = 0.24$.**

vorticity occurs with the bursting of the vortex, but this reversal actually precedes the stagnation point associated with breakdown. Notice also that the vorticity maxima are often not located at the center of the instantaneous streamline roll up. Care must therefore be taken in the interpretation of three-dimensional flows based on these concentrations of vorticity.

The switching of the sign of vorticity is very well explained in terms of the sketches of Fig. 2. Before breakdown, the core of the LEV is straight, but the vortex lines form helices, which on the starboard side of the wing spin clockwise if the observer is looking in the downstream direction as shown in Fig. 2b. If the core is cut by plane $X$, then a component of the vorticity normal to it appears in this plane as counterclockwise above the vortex axis and clockwise below the axis. After breakdown, the core of the vortex forms a corkscrew, which now spirals in the counterclockwise direction again if viewed in the downstream direction. If cut by plane $X$, then vorticity in this plane appears reversed. Another well-known fact now appears to be easier to understand. It is known that along the core of a straight LEV the velocity increases. This group measured in the core of coherent LEVs axial velocities as high as three times the freestream velocity. This is consistent with the sense of the vortex line braid shown schematically in Fig. 2 because the classical Biot Savart law dictates that the azimuthal component of the vorticity induces velocity in the downstream direction. After the onset of breakdown, the corkscrew is spiraling in the opposite direction, and there vorticity induces velocity in the opposite direction. This essentially slows the flow in the center of the broken-down vortex. This can actually lead to reversed flow, a well-known property of breakdown.

## Conclusions

A powerful diagnostic tool was employed to document in great detail the temporal evolution of the flowfield across the breakdown region of a delta wing LEV. Oscillations and corresponding frequencies measured earlier at specific points within the flowfield are now shown to be caused by a specific motion of the vortex core. The core forms a helix, which spirals in the opposite sense than vorticity lines upstream of breakdown. This helix is actually rotating, but the sense of rotation is the same with the sense of vorticity upstream of breakdown. So in simple terms, starboard breakdown resembles a "left-threaded" corkscrew, which is spinning "right," always looking downstream. But at the same time, the helix is stretching in the downstream direction. New evidence also indicates that the spiraling vortex core entrains fluid as indicated by the stable character of the streamlines in the center of the vortex. But this situation is reversed further downstream. The flow now in slowing further and expands at a larger rate. The axial velocity is significantly reduced after the onset of breakdown, and in some places it goes negative, but with helical breakdown there is no consistent volume containing uniformly reversed flow.

## References

[1]Gad-el-Hak, M., and Blackwelder, R. F., "The Discrete Vortices from a Delta Wing," *AIAA Journal*, Vol. 23, No. 6, 1985, pp. 961, 962.

[2]Payne, F. M., Ng, T. T., Nelson, R. C., and Schiff, L. B., "Visualization and Wake Surveys of Vortical Flow over a Delta Wing," *AIAA Journal*, Vol. 26, No. 1, 1988, pp. 137–143.

[3]Lowson, M. V., "The Three Dimensional Vortex Sheet Structure on Delta Wings," AGARD, Paper 11, Oct. 1988.

[4]Reynolds, G., and Abtahi, A., "Instabilities in Leading-Edge Vortex Development," AIAA Paper 87-2424, 1987.

[5]Payne, F. M., "The Structure of Leading Edge Vortex Flows Including Vortex Breakdown," Ph.D. Dissertation, Univ. of Notre Dame, South Bend, IN, 1987.

[6]Washburn, A. E., and Visser, K. D., "Evolution of Vortical Structures in the Shear Layer of Delta Wings," AIAA Paper 94-2317, 1994.

[7]Schaeffler, N. W., "All the Kings Horses: The Delta Wing Leading-Edge Vortex System Undergoing Vortex Breakdown: A Contribution to Its Characterization and Control Under Dynamic Conditions," Ph.D. Dissertation, Dept. of Engineering Science and Mechanics, Virginia Polytechnic Inst. and State Univ., Blacksburg, VA, April 1998.

[8]Gursul, I., and Yang, H., "On Fluctuations of Vortex Breakdown Location," *Physics of Fluids*, Vol. 7, No. 1, 1995, pp. 229–231.

[9]Rediniotis, O. K., "The Transient Development of Vortices Over Delta Wings," Ph.D. Dissertation, Dept. of Engineering Science and Mechanics, Virginia Polytechnic Inst. and State Univ., Blacksburg, VA, 1992.

[10]Rediniotis, O. K., Stapountzis, H., and Telionis, D. P., "Vortex Shedding over Delta Wings," *AIAA Journal*, Vol. 31, 1993, pp. 1555–1562.

[11]Faler, J. H., and Leibovich, S., "An Experimental Map of the Internal Structure of a Vortex Breakdown," *Journal of Fluid Mechanics*, Vol. 86, Pt. 2, 1978, pp. 313–335.

[12]Gursul, I., "Unsteady Flow Phenomena over Delta Wings at High Angle-of-Attack," *AIAA Journal*, Vol. 32, No. 2, 1994, pp. 225–231.

[13]Atta, R., and Rockwell, D., "Leading Edge Vortices due to Low Reynolds Number Flow past a Pitching Delta Wing," *AIAA Journal*, Vol. 28, No. 6, 1990, pp. 995–1004.

[14]Brown, G. L., and Lopez, J. M., "Axisymmetric Vortex Breakdown Part II: Physical Mechanisms," *Journal of Fluid Mechanics*, Vol. 221, 1990, pp. 553–576.

[15]Althaus, W., and Brucker, C., "Study of Vortex Breakdown by Particle Tracking Velocimetry (PTV), Part I: Bubble-Type Vortex Breakdown," *Experiments in Fluids*, Vol. 13, 1992, pp. 339–349.

[16]Towfighi, J., and Rockwell, D., "Instantaneous Structure of Vortex Breakdown on a Delta Wing via Particle Image Velocimetry," *AIAA Journal*, Vol. 31, No. 6, 1993, pp. 1160–1162.

[17]Lin, J.-C., and Rockwell, D., "Transient Structure of Vortex Breakdown on a Delta Wing," *AIAA Journal*, Vol. 33, No. 1, 1995, pp. 6–12.

[18]Visbal, M. R., "Computational and Physical Aspects of Vortex Breakdown on Delta Wings," AIAA Paper 95-0585, Jan. 1995.

[19]Visbal, M. R., "Onset of Vortex Breakdown Above a Pitching Delta Wing," *AIAA Journal*, Vol. 32, No. 8, 1994, pp. 1568–1575.

[20]Cipolla, K. M., and Rockwell, D., "Instantaneous Crossflow Topology on a Delta Wing in Presence of Vortex Breakdown," *Journal of Aircraft*, Vol. 35, No. 2, 1998, pp. 218–223.

[21]Menke, M., Yang, H., and Gursul, I., "Experiments on the Unsteady Nature of Vortex Breakdown over Delta Wings," *Experiments in Fluids*, Vol. 27, No. 3, 1999, pp. 262–272.

[22]Özgören, M., Sahin, B., and Rockwell, D., "Vortex Structure on a Delta Wing at High Angle of Attack," *AIAA Journal*, Vol. 40, No. 2, 2002, pp. 285–292.

[23]Willert, C. E., and Gharib, M., "Digital Particle Image Velocimetry," *Experiments in Fluids*, Vol. 10, 1991, pp. 181–193.

[24]Westerweel, J., "Fundamentals of Digital Particle Image Velocimetry," *Measurement Science and Technology*, Vol. 8, 1997, pp. 1379–1392.

[25]Huang, H. T., and Gharib, M., "Processing Error in Digital Particle Image Velocimetry," FEDSM97-3068, 1997.

[26]Angui, J., and Jimenez, J., "On the Performance of Particle Tracking," *Journal of Fluid Mechanics*, Vol. 185, 1987, pp. 447–468.

[27]Rockwell, D., "Three Dimensional Flow Structure on Delta Wings at High Angle-of-Attack: Experimental Concepts and Issues," AIAA Paper 93-0550, 1993.

[28]Klute, S. M., "The Development and Control of Axial Vortices over Swept Wings," Ph.D. Dissertation, Dept. of Engineering Science and Mechanics, Virginia Polytechnic Inst. and State Univ., Blacksburg, VA, 1999.

[29]Rediniotis, O. K., Klute, S. M., Hoang, N. T., and Telionis, D. P., "Pitch-Up Motions of Delta Wings," *AIAA Journal*, Vol. 32, No. 4, 1994, pp. 716–725.

[30]Rediniotis, O. K., Stapountzis, H., and Telionis, D. P., "Periodic Vortex Shedding over Delta Wings," *AIAA Journal*, Vol. 31, No. 9, 1993, pp. 1555–1562.

[31]Brucker, C., "Study of Vortex Breakdown by Particle Tracking Velocimetry (PTV), Part II: Spiral-Type Vortex Breakdown," *Experiments in Fluids*, Vol. 14, 1993, pp. 133–139.

R. Lucht
*Associate Editor*